Hindawi
International Journal of Polymer Science
Volume 2023, Article ID 7185367, 13 pages
https://doi.org/10.1155/2023/7185367

Research Article

Preparation and Characterization of Polyurethane Rigid Foam Nanocomposites from Used Cooking Oil and Perlite

Muntajab Sarim, Mir Mohammad Alavi Nikje, and Maryam Dargahi

Department of Chemistry, Faculty of Science, Imam Khomeini International University (IKIU), Qazvin, Iran

Correspondence should be addressed to Mir Mohammad Alavi Nikje; drmm.alavi@gmail.com

Received 10 July 2022; Revised 12 October 2022; Accepted 14 March 2023; Published 11 April 2023

Academic Editor: Cornelia Vasile

Modern chemical industries trend towards industrial ecology to achieve a circular economy, because of increasing environmental and economic awareness jointly. One of the most important of these industries is polyurethane, accompanied by more and more interest in using renewable polyols. The study focuses on synthesizing and characterizing polyurethane rigid foams formulated by replacing 40%, 60%, and 100% of a petrochemical polyol with a bio-polyol derived from used cooking oil, and introducing perlite and modified perlite nanoparticles into the bio-polyol. The products were evidenced by transmission electron microscopy (TEM), Fourier transform infrared (FTIR), nuclear magnetic resonance spectral analyses, thermogravimetric analysis (TGA), and scanning electron microscopy equipped with energy-dispersive spectroscopy. The results indicate that the hydroxide value and viscosity at 25°C of the bio-polyol were around 456 ± 30 mg KOH/g and 148 mPa s. Bio-polyol blends of 40% and 60% had no significant effect on the thermal properties of polyurethane systems. The lowest value of char yield was observed for the sample with a 100% bio-polyol content of 2.3%. The beneficial effects of both perlite and modified perlite particles on the 100% bio-polyol-based foam were observed as having an effective role in improving thermal stability and reconstructing cellular structure. The yield char increased to 13.2%, 14%, 14.7%, and 15% for the two filler contents 2.5% and 5%. However, the new bio-polyol has a fairly good value in industrial construction, and the perlite particles have enhanced and improved this value.

1. Introduction

Polyurethanes as the special group of heterochain polymers characterized by the structural unit urethane groups –NH–COO–, which are esters of carbamic acid and synthesized by reacting a polyol with a diisocyanate in the presence of catalysts, as well other desired additives. The wide range of polyurethanes usages in various industries depends mainly on the molecular weight and functionality of oligo polyol, which allows the final products to adapt and resolve difficult problems and form into unusual shapes [1–3]. Moreover, the growth of polyurethane rigid foam (PURF), especially in the world experiencing expansion in the construction and furniture sector, can be attributed to its different properties such as strong mechanical strength, sound, and thermal insulation, which make it suitable for harsh weather environmental conditions and useable in large quantities globally [4, 5]. In this regard, generally, crude oil is supplied as the main resource in the production of polyurethane raw materials namely, polyols, isocyanates, etc. Recently, due to commercial and environmental trends, environmentally benign raw ingredients such as vegetable oils and some feedstocks such as waste cooking oil or used cooking oil (UCO) have been noticed for polyurethane manufacturing [6].

UCO constitutes one of the most dangerous wastes that threaten the environment, especially that its quantities are large and cannot be ignored, as its disposal in sewage leads to major problems in the sewage network in general, such as narrowing the flow section [7, 8]. This results in the formation of anaerobic conditions, irritating odors, poisoning of the water medium, and poisoning of treatment. In particular, at treatment plants, a thin impermeable layer is formed, which prevents the exchange of gaseous with air that results in increasing wastewater pollution indicators (Biochemical Oxygen Demand (BOD), Chemical Oxygen Demand (COD), Total Suspended Solids (TSS)), and a reduction of

the efficiency of pumps and filters at the station [9, 10]. The recent increase in the number of publications and patents underlines the enormous potential that UCO (when recycling) goes beyond its use only in the production of biofuels, as it can be used as value-added green chemicals such as surfactants [11, 12], binders for building blocks [13], plasticizers [14, 15], lubricants [16], and biopolymers [17]. Environmentally being polyols, which naming as biopolymers, can be obtained from either transesterification of oils or ring-opening of epoxidized oils processes by using a wide range of reactive materials such as alcohols in wide ranges of hydroxyl numbers as well functionalities and viscosities [18]. For instance, the hydroxyl number and viscosity of the biopolyol obtained from the ring-opening reaction of epoxidized rapeseed oil with 1,6-hexanediol were (250 mg KOH/g, 5128 mPa s) more than twice as high as that of the biopolyol obtained with 1-hexanol (104 mg KOH/g, 643 mPa s) [19], whereas those produced from the transesterification of rapeseed oil with diethanolamine (DEA), triethanolamine, and glycerol were higher than (1000 mg KOH/g) the formers [20]. Regarding ring-opening of epoxidized UCO with diethylene glycol, the hydroxyl number was 139.6 and 159.2 mg KOH/g with viscosity 3275 and 961 mPa s by using two types of catalysts namely, tetra-fluoroboric acid and sulfuric acid [21]. As for the transesterification of UCO with agents (ethylene glycol, propylene glycol, diethylene glycol, glycerin, and triethanolamine), Kurańska and Malewska [22] concluded that alcohols containing two primary hydroxyl groups were more reactive than alcohols containing three hydroxyl groups or two hydroxyl groups including one primary and one secondary group, and the most reactive agent was triethanolamine.

Generally, the catalyst plays a key role in designing and making a process successful. Magnetic nanoparticle catalysts (MNPs) are considered a turning point in the world of catalysts, especially in organic synthesis, because they have advantages in terms of sustainability and cleaner production, as they are non-toxic and can be recovered and used again. Some of their disadvantages can also be overcome by improving surface properties and selectivity. In parallel, ionic liquids (ILs) have been witnessed in recent years great interest as environmentally friendly solvents due to their specific properties such as high thermal stability, non-flammability, neglected vapor pressure, and the ability to dissolve a wide range of materials, but they have suffered from their limited practical application due to the presence of some drawbacks such as high viscosity, the difficulty of separating from the reaction phase and being reused. To overcome the disadvantages of the previous two types, it was possible to combine the positive properties of each of them by combining them through bridge moiety and forming the IL magnetic nanoparticles (MNPs) catalysts [23–25].

On the other hand, in the nanocomposites field, researchers have tended to incorporate inorganic fillers such as clay minerals, particularly, nano ones into polymeric materials to improve the polymer properties. For example, adding nanoclay in low quantities to polyurethane improves significantly thermal, mechanical, and other properties [26]. The researchers also saw that to improve the process of incorporating the nanoclay into the polymer matrix, its surface can be modified with hydrophobic organic materials such as quaternary amine salts and others. Among the most important fillers used in this field are bentonite, vermiculite, colosite, and perlite [27]. Perlite is a naturally occurring mineral, which is inexpensive and available. It is usually used with cement to increase thermal insulation. However, it does not achieve the desired levels, absorbs water, is more susceptible to shear forces, and breaks easily when mixed [28]. Perlite contributes to solving the polyurethane problem by increasing the thermal stability, mechanical strength, and reducing flammability, and at the same time, improving the thermal insulation properties of perlite products [29].

In this work, PURFs were fabricated from blending UCO-based polyol with commercial polyol at different weight ratios of 40%, 60%, and 100%. More, perlite and modified perlite were introduced to the 100% bio-polyol-based foam at different weight ratios of 2.5% and 5%. The thermal and morphological properties of PURFs formulated were investigated. It is noteworthy that novel bio-polyol was synthesized from epoxidation reaction of UCO, then oxirane ring-opening by DEA by using magnetic nano-catalyst.

2. Experimental

2.1. Materials. Dalto Foam TA® 14,066 polyether polyol (viscous yellow liquid, viscosity: 5260 cps at 25°C and water content: 2.3%) containing additives and methylene diphenyl diisocyanate (MDI) (SuprasecVR 5005, dark brown liquid, viscosity: 220 cps at 25°C) for rigid PU foam formulation were purchased from Huntsman company. Iron (II) chloride tetrahydrate (99.7%), iron (III) chloride hexahydrate (99.0%), ammonia (25%), ethanol (99.7%), 1-methyl imidazole, sodium tetrafluoroborate, glacial acetic acid (99.9 wt.%), hydrogen peroxide (30 wt.%), hydrochloric acid (37%), sodium hydroxide, and tetra-*n*-butyl ammonium bromide (TBAB) were purchased from Merck. 3-chloropropyltrimethoxy silane was purchased from Sigma. Perlite with chemical composition (%) (SiO_2: 74.66%, Al_2O_3: 13.66%, Fe_2O_3: 0.69%, CaO: 0.42%, Na_2O: 3.34%, K_2O: 5.36%, MgO: 0.32%, TiO_2: 0.164%, MnO: 0.092%, P_2O_5: 0.024%, S: 0.009%, and L.O.I: 1.12%) was purchased from Alvand company, Qazvin, Iran. UCO (OH value ~1.73 mg KOH/g, yellow liquid viscosity ~67 mPa s.) was collected from restaurants in Qazvin, Iran.

2.2. Instrument. ^{1}HNMR spectra were performed in a Bruker 300 nuclear magnetic resonance instrument, using deuterated chloroform ($CDCl_3$) as solvent. FT-IR spectra (400–4000 cm^{-1}) were carried out on a Bruckner Tensor 27 spectrophotometer. Viscosity (η) was determined at 25°C using a rotational rheometer (Rheolab QC, Anton Paar). Thermogravimetric analysis (TGA) was done with Perkin-Elmer Pyris Diamond TG/DTA under air atmosphere at a heating rate of 7.5°C/min. To disperse the nanoparticles, an ultrasonic homogenizer (Hielscher, UP200S, Germany) was used. Field Emission Scanning Electron Microscopy (FESEM) and transmission electron microscopy (TEM) tests were obtained by FE-SEM ZEISS Sigma 300 and TEM Philips EM 208S, respectively.

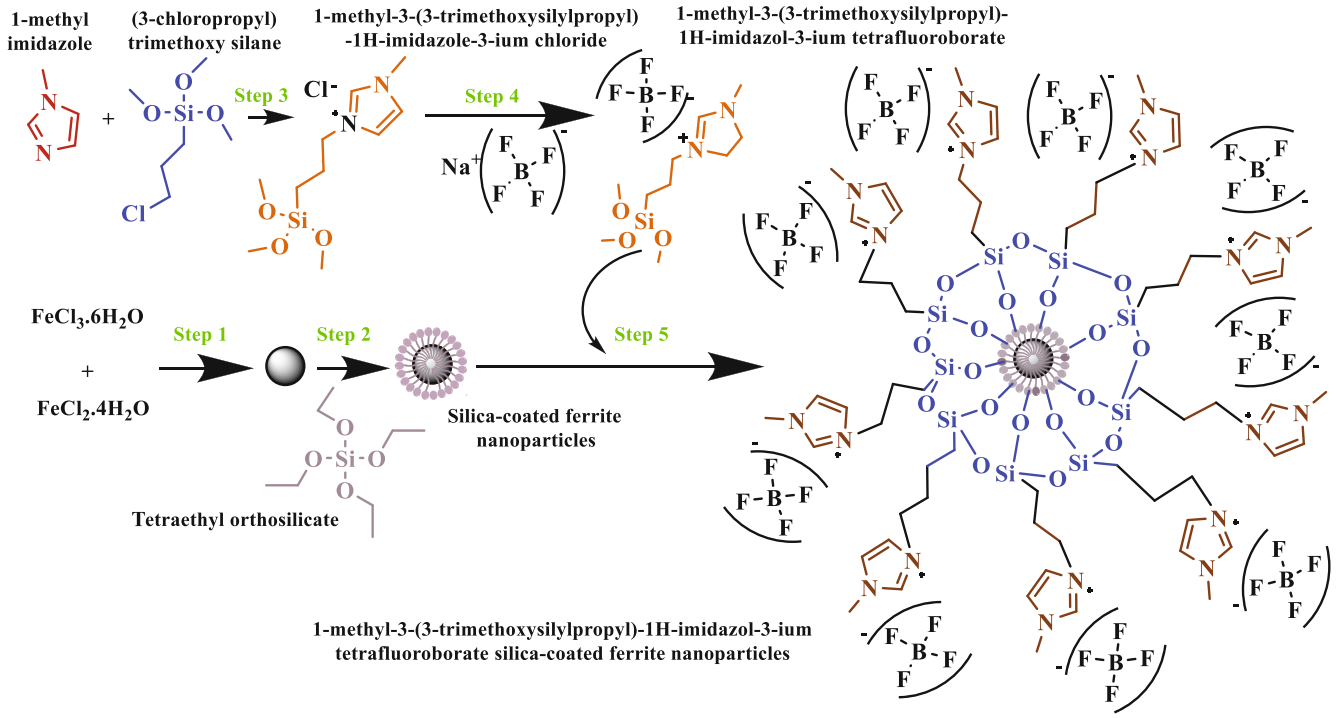

Figure 1: The catalyst synthesis steps.

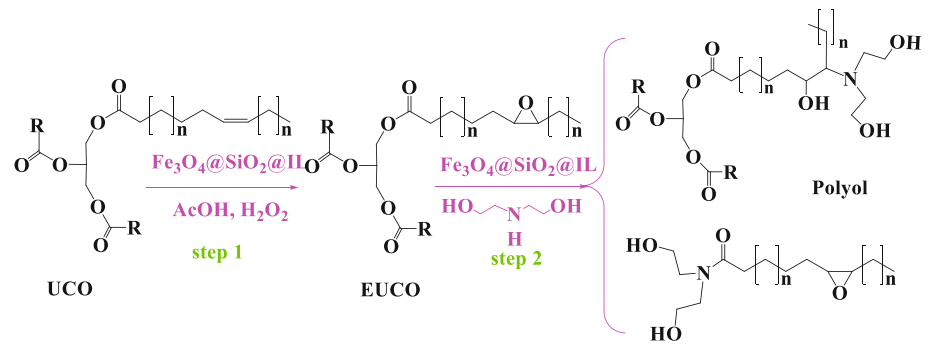

Figure 2: EUCO and EUCO-based polyol synthesis.

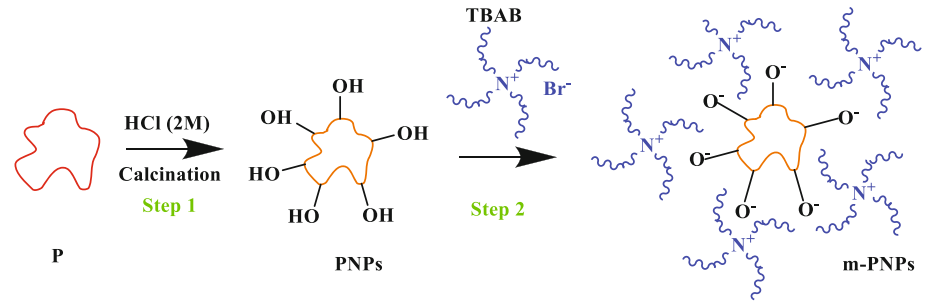

Figure 3: Modified perlite nanoparticles synthesis steps.

2.3. Fe_3O_4@SiO_2@IL Catalyst Synthesis Procedure. The catalyst was prepared using as described in the literature [30–34] (Figure 1), with some modifications.

2.3.1. Synthesis of Ferrite Nanoparticles. The MNPs were carried by dissolving $FeCl_3.6H_2O$ (11.68 g) and $FeCl_2.4H_2O$ (4.30 g) in deionized water (200 ml) at 70°C for 20 hours, and then $NH_3.H_2O$ (20 ml, 25%) was added with vigorous stirring.

2.3.2. Synthesis of Silica-Coated Ferrite Nanoparticles. The magnetite precipitates were separated and washed several

Table 1: Codes of PURFs from commercial polyol and novel polyol with different ratios.

Commercial polyol (%)	100	60	40	0
Synthesized polyol (%)	0	40	60	100
PURF code	PU-S1	PU-S2	PU-S3	PU-S4

Table 2: Codes of prepared PURF nanocomposites.

Synthesized polyol (%)	100	100	100	100	100
PNP (%)	—	2.5	5	—	—
m-PNP (%)	—	—	—	2.5	5
PURF code	PU-S4	PU-S4-1	PU-S4-2	PU-S4-3	PU-S4-4

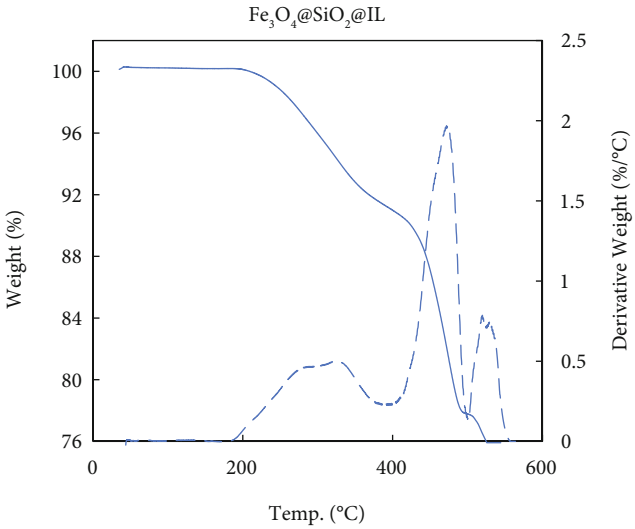

Figure 4: TGA-DTG of Fe_3O_4@SiO_2@IL.

times with deionized water and dried at 70°C all night. MNPs (1 g) were dispersed in a solution mixture of ethanol (400 ml) and deionized water (100 ml) under ultrasonication for 15 minutes. Then ammonium hydroxide solution (15 ml, 25%) was added followed by the addition of tetraethyl orthosilicate (10 ml) with stirring at 25°C for 20 hours. The product was washed with water several times and dried under a vacuum.

2.3.3. Synthesis of 1-Methyl-3-(3-Trimethoxysilylpropyl)-1H-Imidazole-3-Ium Tetrafluoroborate. 1-Methyl-3-(3-trimethoxysilylpropyl)-1H-imidazole-3-ium chloride was prepared by refluxing 1-methylimidazole (20 ml, 0.25 mol) and (3-chloropropyl) trimethoxy silane (46 ml, 0.25 mol) at 80°C for 120 hours followed by washing the product with diethyl ether and heating under vacuum. The IL with fluoroborate anion was prepared by dissolving 1-methyl-3-(3-trimethoxysilylpropyl)-1H-imidazole-3-ium chloride (50 mmol) in acetonitrile (300 ml) followed by addition of sodium tetrafluoroborate (50 mmol) and stirring for 120 hours at 30°C, then the solvent evaporated

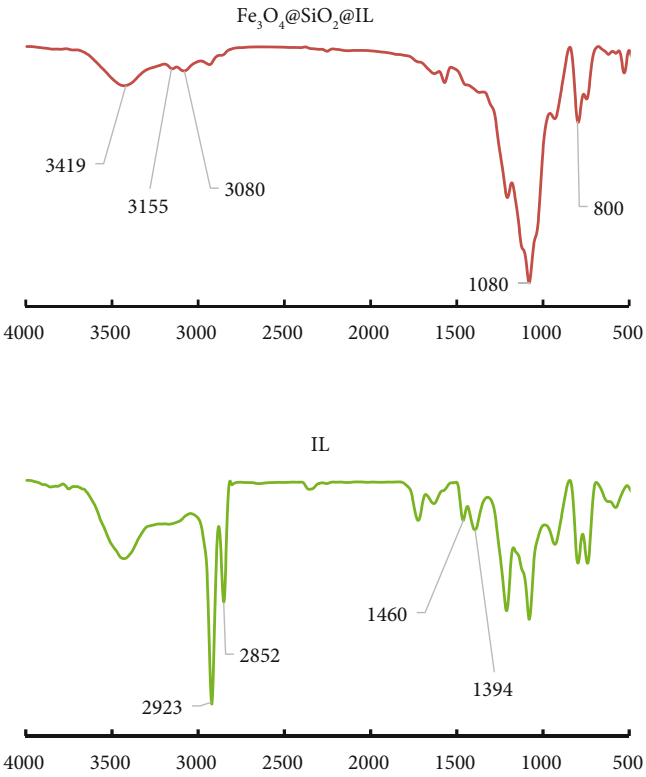

Figure 5: FTIR of IL and Fe_3O_4@SiO_2@IL.

under vacuum, the precipitate filtered, washed with dichloromethane (100 ml) three times, and dried under vacuum at room temperature.

2.3.4. Synthesis of 1-Methyl-3-(3-Trimethoxysilylpropyl)-1H-Imidazol-3-Ium Tetrafluoroborate Silica-Coated Ferrite Nanoparticles. Silica-coated ferrite nanoparticles (0.5 g) were dispersed in toluene by ultrasonication. Then, 1-methyl-3-(3-trimethoxysilylpropyl)-1H-imidazole-3-ium tetrafluoroborate (5 g) was added to the mixture and stirred at 90°C for 24 hours. The product was isolated, washed with acetonitrile (100 ml) and methanol (100 ml) twice, and dried under a vacuum.

2.4. EUCO and EUCO-Based Polyol Synthesis Procedure. For the epoxidation reaction, 100 g of UCO, 15 g of acetic acid, 35 g of hydrogen peroxide, and the catalyst were added to the refluxed three-necked round bottom flask at 80°C and continued stirring for 6 hours. The organic phase was washed with warm water and distilled to be free of acid and water. The procedure was completed by placing 50 g of Epoxidized Used Cooking Oil (EUCO) in the same flask and adding 50 g of DEA and catalyst for 10 hours at 90°C. The product was washed with water and extracted with diethyl ether. The two previous processes were carried out by using 1 wt.% of the catalyst (Figure 2). The hydroxyl number of synthesized polyol was calculated according to the method described in the literature and was 456 ± 30 mg KOH/g [35].

2.5. Preparation of Modified Perlite Nanoparticles (m-PNPs). After heating 5 g of perlite (P) to the degree 500°C for 1 hour, it was placed in a refluxed flask, and 150 ml of HCl

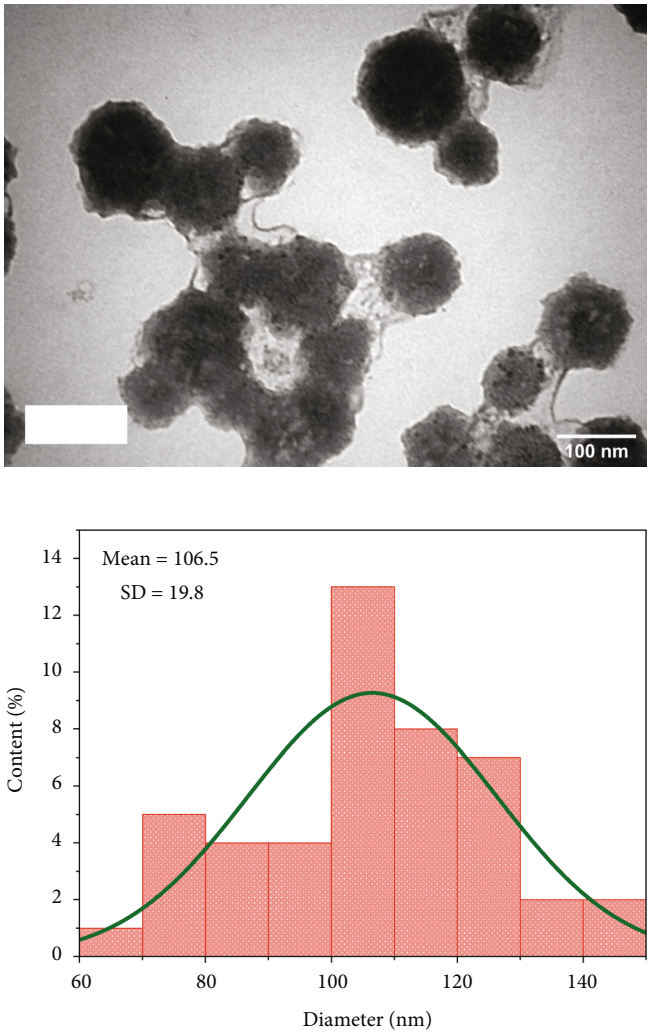

Figure 6: TEM of Fe_3O_4@SiO_2@IL and particles size distribution.

(2 M) was added and left for 24 hours. The product was washed with distilled water and neutralized with sodium hydroxide, then washed again with distilled water and filtered by filter paper under vacuum, then dried in oven at 100°C for 2 hours, and calcinated at 700°C for 1 hour. 1 g of perlite nanoparticles (PNPs) was added to 100 ml, 50% of TBAB in a stirred-refluxed flask at 80°C for 24 hours, the product filtered, and dried vacuum oven at 100°C (Figure 3) [36].

2.6. Preparation Polyurethane Rigid Foam Nanocomposites. The PURFs and their nanocomposites were carried out by a one-step process from A and B components. A consists of polyols with different contents of novel polyols (0, 40, 60, and 100 wt.%) for foams and dispersed nano-perlite and modified nano-perlite particles in novel polyol (100 wt.%) by using an ultrasonic homogenizer for nanocomposites. B component (isocyanate) was added to the system, mixed mechanically in an open mold, and kept for 24 hours at room temperature (Tables 1 and 2) [37, 38].

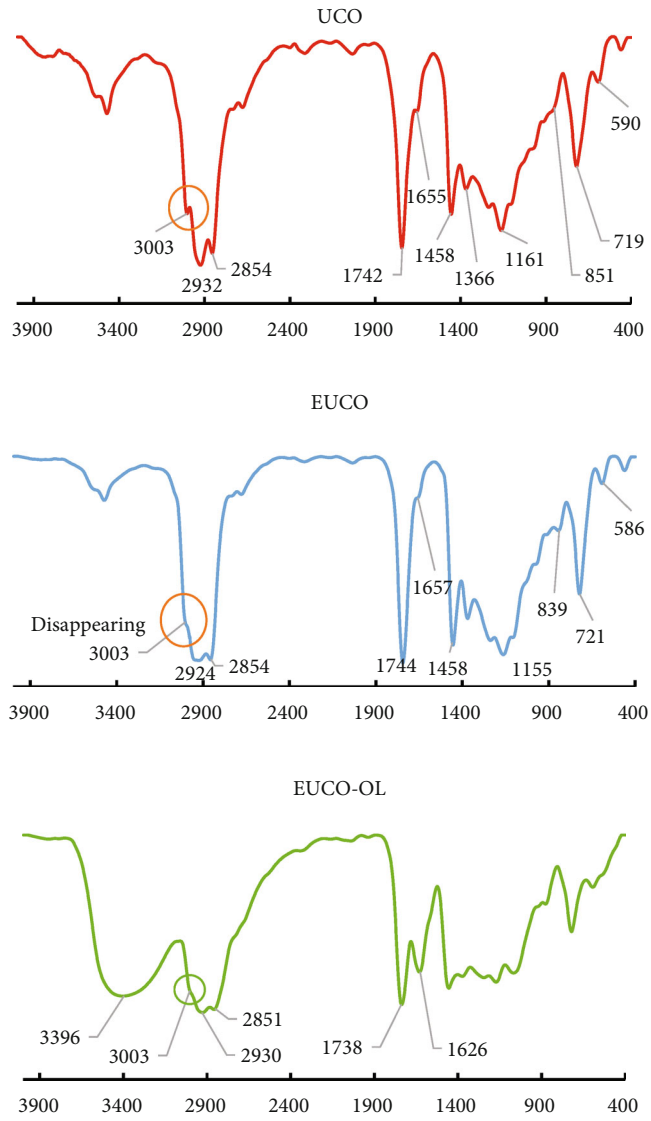

Figure 7: UCO, EUCO, and EUCO-OL FTIR spectra.

3. Results and Discussion

3.1. Catalyst Analysis

3.1.1. TGA-DTG Analysis. The Thermogravimetric analysis/Derivative Thermogravimetry (TG/DTG) curve of the catalyst shows three degradation steps in temperature ranges of 200–385°C, 385–500°C, and 500–550°C, with gradual weight loss of about 8.72%, 13.67%, and 3.63%, respectively. The first step can be attributed to the loss of organic groups of 1-methyl-3-(3-trimethoxysilylpropyl)-1H-imidazole-3-ium tetrafluoroborate. While the second step could be due to the loss of the remaining previous organic groups and SiO_2/Fe_3O_4, the last one may indicate the phase change of the MNPs. The graph also indicates the high thermal stability added by the presence of IL groups on the silica layer, as it can be used in organic reactions up to 200°C (Figure 4) [30, 31].

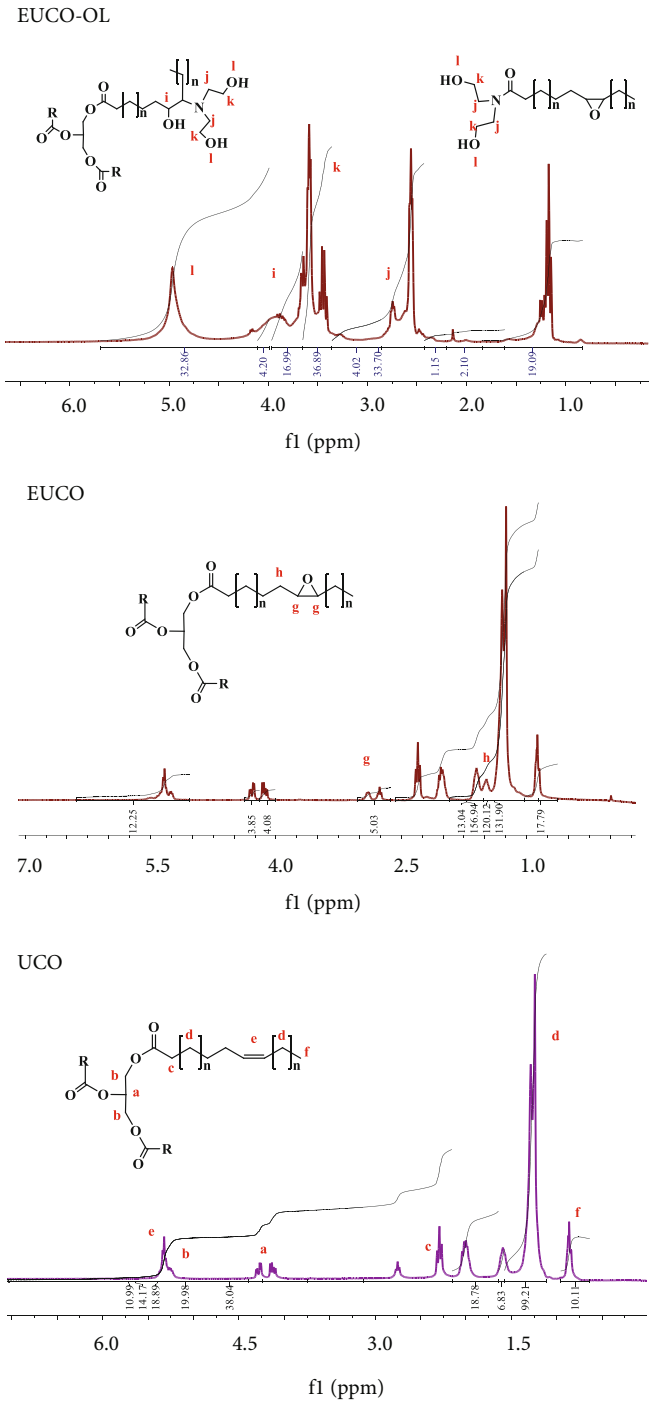

Figure 8: UCO, EUCO, and EUCO-OL ^{1}HNMR spectra.

3.1.2. FTIR Analysis. Figure 5 shows the Fourier-transform infrared (FTIR) spectra of IL and Fe_3O_4@SiO_2@IL. The important bonds are Fe–O–Si (800 cm^{-1}), Si–O–Si (1080 cm^{-1}), C–H stretching vibrations of the imidazolium ring (3080, 3147 cm^{-1}), Si–OH (3429 cm^{-1}), CH_3, CH_2 stretching vibrations (2922 cm^{-1}, 2852 cm^{-1}), respectively, and CH_3, CH_2 bending vibrations (1463 cm^{-1}, 1396 cm^{-1}). The results provided that ILs were successfully attached to the surface of MNPs coated with a silica shell [36].

3.1.3. TEM Analysis. The TEM of the IL MNPs presented in Figure 6 has been evaluated for morphologies and sizes of the nanoparticles. The results show that the diameter average is 106.5 ± 19.8 nm, and the degrees of core–shell darkening in colors show the main layers, which are Fe_3O_4, SiO_2, and IL [37].

3.2. EUCO and EUCO-Based Polyol Analysis

3.2.1. FTIR Analysis. The epoxidized oil and the polyol were detected in UCO, EUCO, and EUCO-OL FTIR spectra

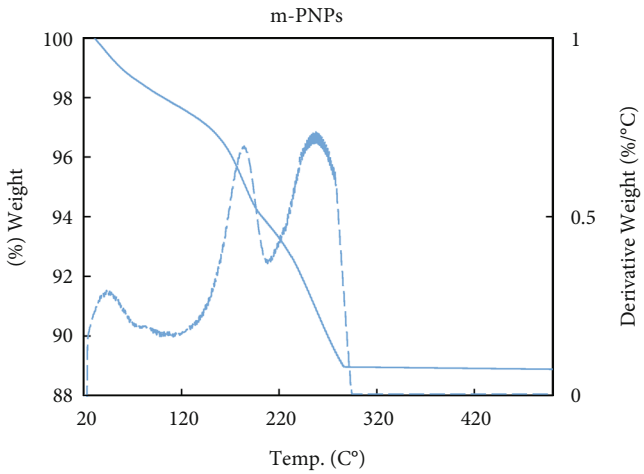

Figure 9: TGA-DTG of m-PNPs.

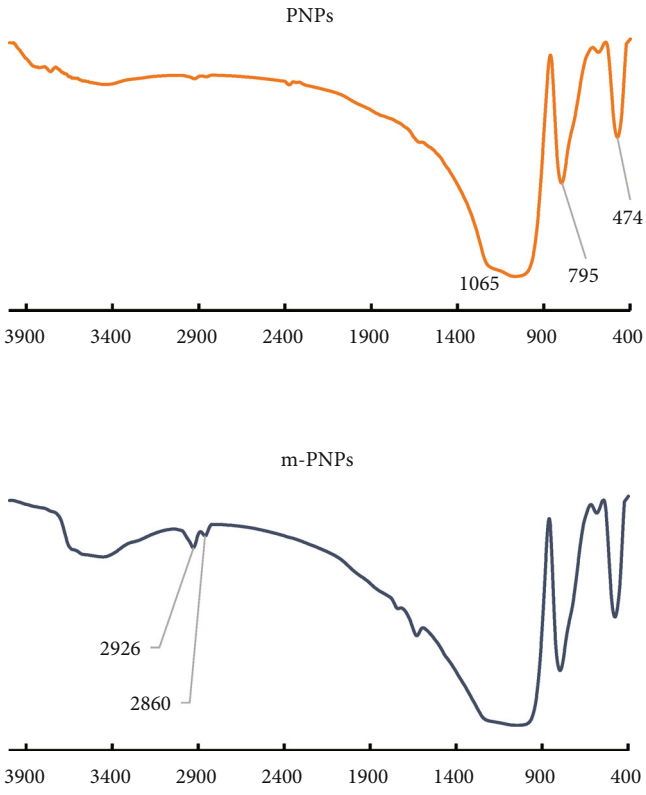

Figure 10: PNPs and m-PNPs FTIR spectra.

(Figure 7). The intensity of peek in the UCO spectrum at 3003 cm^{-1} corresponded to C–H of alkene was decreased and disappeared in the EUCO spectrum, accompanied by appearing a peek at 845 cm^{-1} corresponded to oxirane ring. Moreover, a broad hydroxyl band appeared at 3400 cm^{-1}), and peek at 1632 cm^{-1} corresponded to tertiary amide in the EUCO-OL spectrum, which indicated that there was an amidification reaction that competes the ring-opening reaction. Generally, there are participated peeks in the three spectra such as C=O stretching vibrations at 1745 cm^{-1}, –CH_3 asymmetrical stretching at 2922 cm^{-1} and symmetrical bending at 1370 cm^{-1}, –CH_2 asymmetrical stretching at 2852 cm^{-1} and scissoring at 1456 cm^{-1}, C=O Fermi resonance at 2678 cm^{-1}, –OH stretching vibrations of hydroperoxide, bending of C–O bands at 1240, 1160, 1108 cm^{-1}, and –$(CH_2)_n$– rocking at 722 cm^{-1}.

3.2.2. ^{1}HNMR Analysis. The ^{1}HNMR spectra illustrated some changes in the signals. The emergence of new areas in the range of 2.8–3 ppm belonging to the hydrogens attached to the oxirane ring in the spectrum of EUCO coincided with the partial disappearance of some others in the range of 5.4–5.5 ppm belonging to the olefinic hydrogens in the spectrum of UCO. The yield of the epoxidation reaction can be calculated, the areas (A), by the relationship (1):

$$\text{Yield} = \left(\frac{Ax}{Ax + Ay}\right) \times 100, \quad (1)$$

where x and y were in the range of 2.8–3 ppm and 5.3–5.4 ppm, respectively. Results of data showed that epoxidation yield was 50%. On the other hand, the same areas (2.8–3 ppm) in the EUCO spectrum disappeared completely to show new ones in the range of 3.4–4 ppm in the EUCO-OL spectrum (Figure 8). By using the same relationship: previous relationship (1), with respect x the range (3.4–4 ppm) and y the range (2.8–3 ppm), the yield was 95%, concerning the little amount of catalyst compared with literature [35].

3.3. m-PNP Analysis

3.3.1. TGA-DTG Analysis. The TG/DTG curve of modified perlite nanoparticles (m-PNPs) shows three stages of decomposition. They occur in the ranges 20–130°C, 130–220°C, and 220–310°C, and the loss in mass 2.5%, 4%, and 5.5%, respectively. The first decomposition indicates the hydration of water molecules. The second one can be attributed to ammonium salts and the third to PNPs (Figure 9) [38].

3.3.2. FTIR Analysis of m-PNPs. The PNPs and m-PNPs FTIR spectra showed Si–O vibrations at 474 cm^{-1}, Si–O–Si symmetrical vibrations at 798 cm^{-1}, broadband correspond to Si–O–Si unsymmetrical vibrations at 1053 cm^{-1}, –OH at 3430 cm^{-1}, and CH_3, CH_2 stretching vibrations at 2928 cm^{-1}, 2854 cm^{-1}), respectively, in m-PNPs spectra (Figure 10).

3.3.3. TEM Analysis of m-PNPs. To study the morphology of nanomaterials, TEM technology was used. As can be seen in the image, the modified perlite particles have a diameter average of 206 ± 143 nm and are somewhat agglomerated. Nevertheless, the core–shell structure is with light contrast of tetra-*n*-butyl ammonium shell and dark contrast cores are of PNPs (Figure 11) [37].

3.4. Polyols and PURF Characterization

3.4.1. TGA-DTG Analysis. TGA analysis was performed for commercial and synthesized polyols (Figure 12, Table 3). The synthesized polyol was found to have a lower

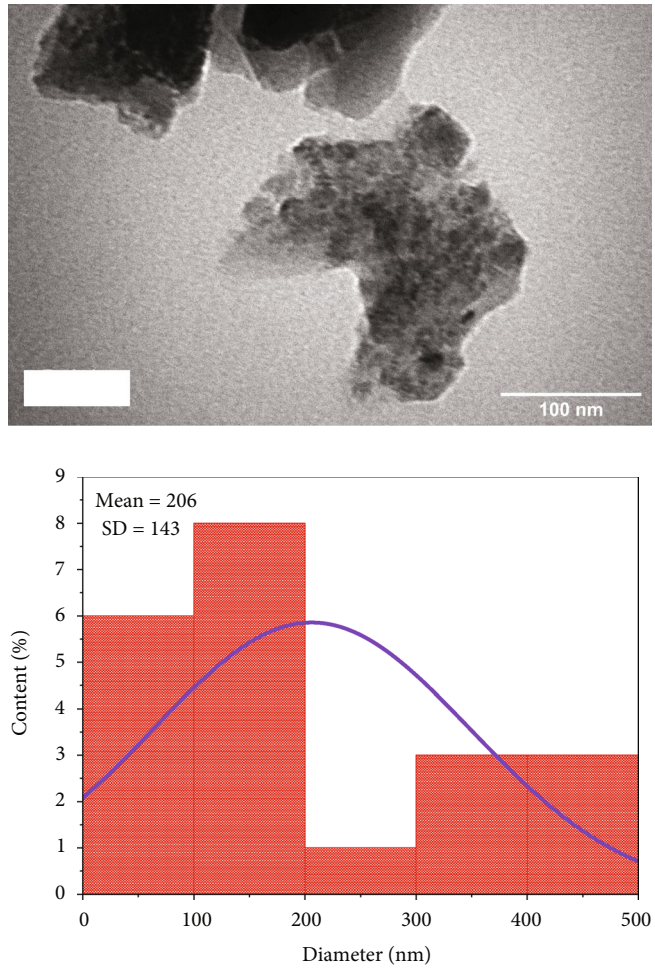

Figure 11: TEM of m-PNPs and particles size distribution.

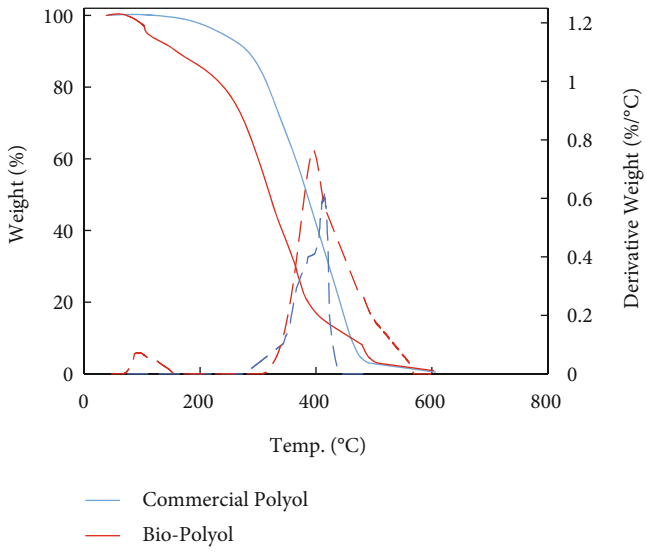

Figure 12: TGA-DTG of commercial and synthesized polyols.

Table 3: Summary of TGA results for polyols.

Code	$T_{5\%}$ (°C)	$T_{50\%}$ (°C)	T_{max1} (°C)	T_{max2} (°C)	Char yield (%)
Com. Polyol	236	385	—	412	0
Bio-polyol	100	320	109	395	0

temperature loss of 50% and maximum degradation compared to the commercial polyol. In the case of bio-polyol, a weight loss at 100°C may correspond to the water evaporation. The second one occurred at maximum degradation of 395°C. This temperature range may relate to polyester decomposition [39].

The results of the thermal degradation analysis of PURFs are summarized in Figure 13 and Table 4. The temperatures of loss weight 5% and 50% are $T_{5\%}$ and $T_{50\%}$ as well as the maximum degradation rates are T_{max1} and T_{max2}. The PU-S1 exhibited two degradation steps: the first one was in the temperature range of 200–400°C, with a weight loss of

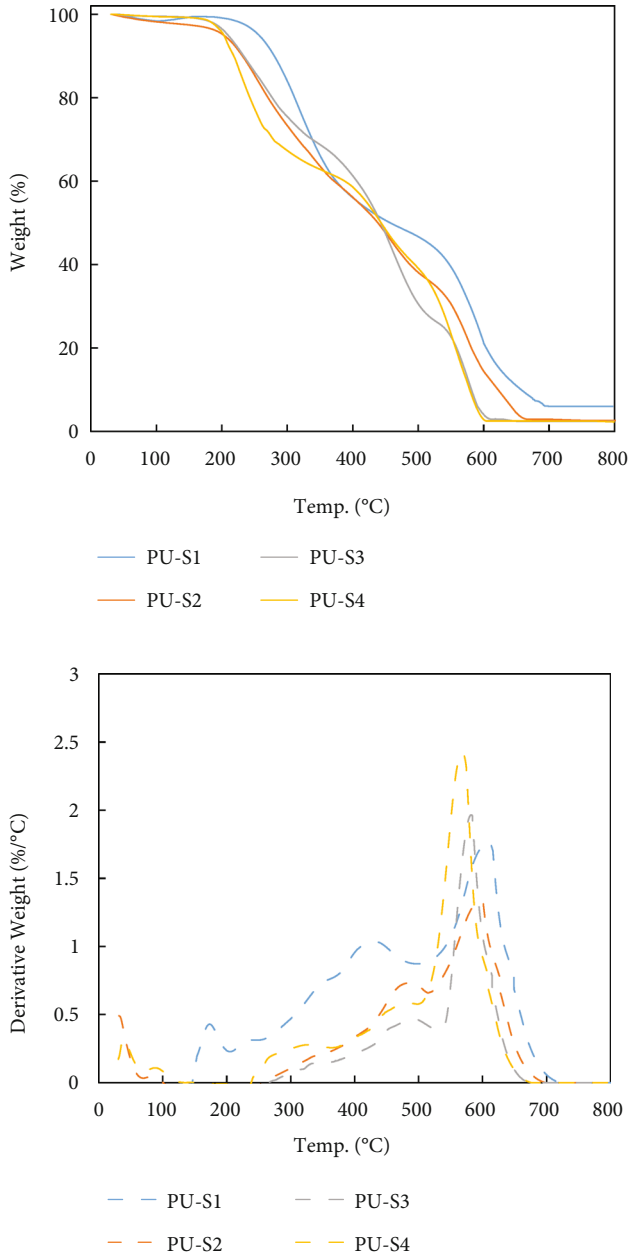

Figure 13: TGA-DTG of PURFs.

Table 4: Summary of TGA results for PURFs.

Code	$T_{5\%}$ (°C)	$T_{50\%}$ (°C)	T_{max1} (°C)	T_{max2} (°C)	Char yield (%)
PU-S1	265	457	426	596	6
PU-S2	203	438	487	587	2.6
PU-S3	209	442	487	581	2.4
PU-S4	203	443	483	574	2.3

Table 5: Summary of TGA results for PURF nanocomposites.

Code	$T_{5\%}$ (°C)	$T_{50\%}$ (°C)	T_{max1} (°C)	T_{max2} (°C)	Char yield (%)
PU-S4	203	443	483	574	2.3
PU-S4-1	207	483	490	552	13.2
PU-S4-2	201	474	467	537	14
PU-S4-3	202	501	468	538	14.7
PU-S4-4	200	494	518	552	15

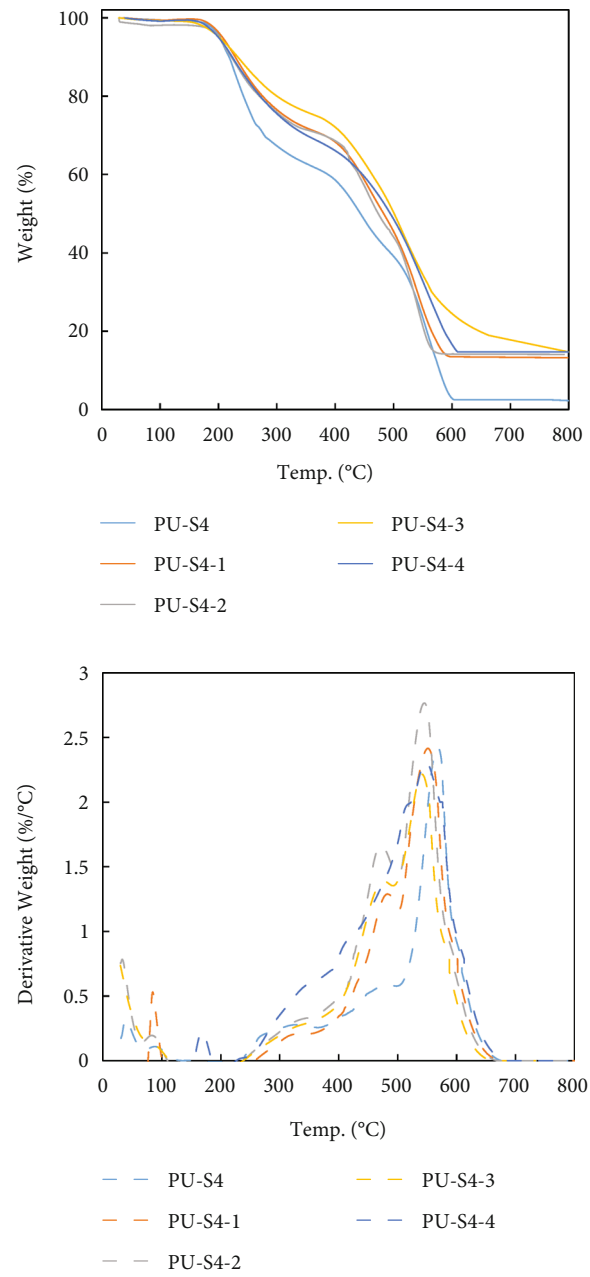

Figure 14: TGA-DTG of PURF nanocomposites.

50%, which can be attributed to the thermal decomposition of urethane and urea bonds in the rigid segments of the PURFs, and the second one in the range 400–700°C, with a weight loss 44%, which may due to the thermal decomposition of the ester bonds in the soft segments and aromatic compound of isocyanates of the PURFs.

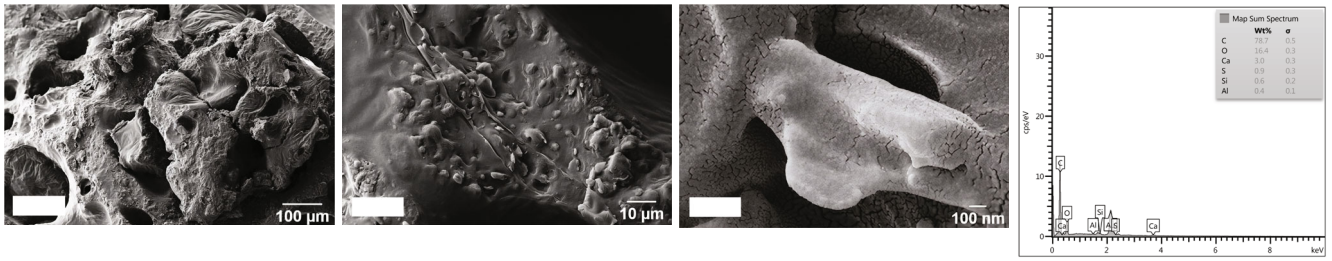

Figure 15: SEM images and energy-dispersive spectroscopy (EDS) analysis of PURFs PU-S4.

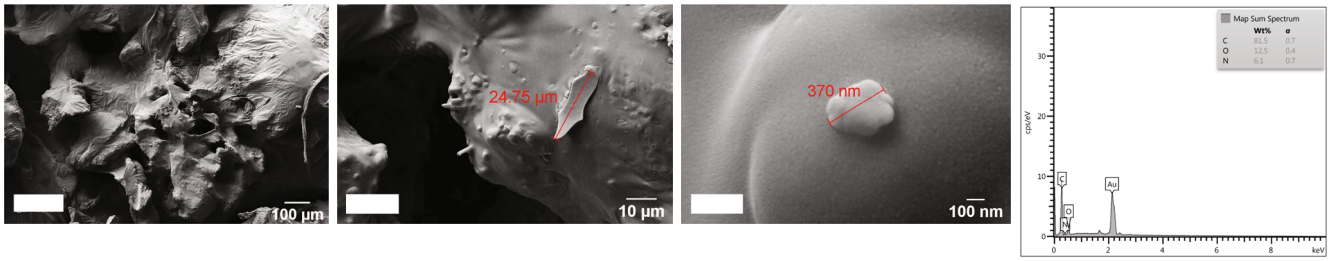

Figure 16: SEM images and energy-dispersive spectroscopy (EDS) analysis of PURFs PU-S4-1.

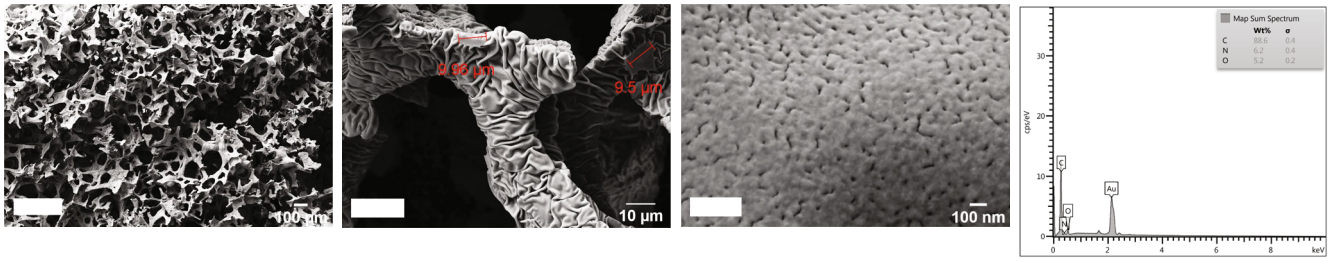

Figure 17: SEM images and energy-dispersive spectroscopy (EDS) analysis of PURFs PU-S4-2.

The introduction of bio-polyol at ratios of 40% and 60% for the fabricated foams may led to some changes in the foam structure and the emergence of an additional stage in the thermal decomposition corresponding to the degradation of the semi-rigid segments. As the bio-polyol content increases, the degree of phase separation in polyurethane foam increases. It probably causes the pyrolysis pathway of the foam to be changed to form a three-phase state. Table 4 shows decreasing in $T_{5\%}$, $T_{50\%}$, and T_{max2} values and increasing in T_{max1} values upon adding the bio-polyol. However, the results indicate that the bio-polyol at ratios 40% and 60% has no significant effect on the thermal degradation process. Surprisingly, the DTG curves assist the statement that increasing the novel bio-polyol content shifts the maximum temperatures towards higher values of 426°C, 487°C, 487°C, and 483°C for PU-S1, PU-S2, PU-S3, and PU-S4, respectively, which means the potential effect may be on the semi-rigid segment was more. In other words, the bio-polyol not only supports the flexible part, because it is based on vegetable oil, but also supports the hard part. In substantiation, the thermal degradation of PU-S4 (100% bio-polyol) shows three stages 150–350°C, 350–480°C, and 480–700°C, with weight loss of 35%, 20%, and 42%, which can be attributed to rigid, semi-rigid, and soft segments, respectively.

The introduction of PNPs and m-PNPs had found a significant effect on the values of $T_{50\%}$, T_{max1}, and T_{max2}, as shown in Table 5 without showing a significant change in the degradation steps. Increasing temperatures of $T_{50\%}$ indicate that in the second step, the active role of PNPs and m-PNPs in impeding heat transfer through the formation of a protective layer begins. Comparing the PNPs with m-PNPs, we note that modification of PNPs with TBAB increases the $T_{50\%}$ values. Excess amounts of nanomaterials (5%) may lead to a heterogeneous distribution in the polymer matrix and consequently to agglomeration and lower thermal stability of these samples. The char residue at 800°C for foam composites was 13.2%, 14%, 14.7%, and 15% for PU-S1, PU-S2, PU-S3, and PU-S4, respectively. The increase in the filler content, the slightly increases residue content. However, this indicates that the thermal stability of foams is improved at higher temperatures (Figure 14) [29, 34, and 37].

3.4.2. FE-SEM Analysis. FE-SEM was used to examine the morphology of PURF nanocomposites and the effect of dispersion of the PNPs and m-PNPs on the PURFs matrix. The PURF nanocomposites were obtained by brittle fracture. The fracture surface of the PU based on bio-polyol (PU-S4) is presented in Figure 15 while the fracture surfaces of PU/

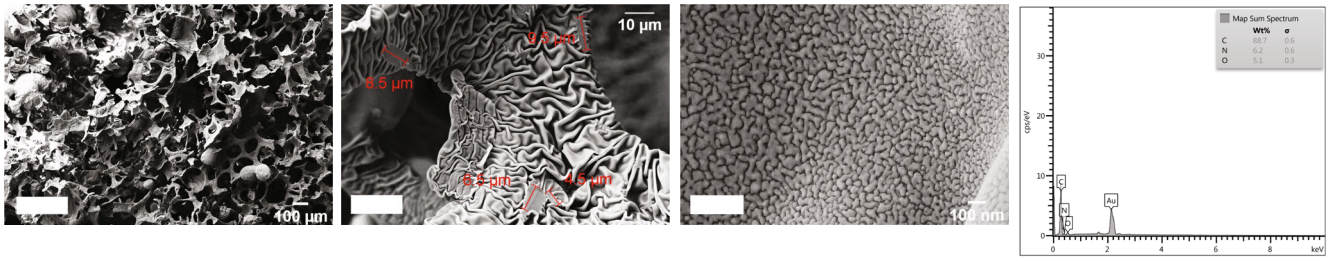

Figure 18: SEM images and energy-dispersive spectroscopy (EDS) analysis of PURFs PU-S4-3.

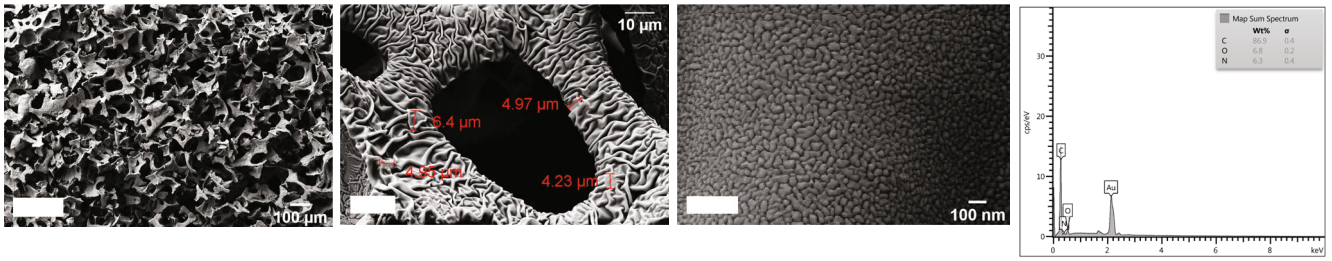

Figure 19: SEM images and energy-dispersive spectroscopy (EDS) analysis of PURFs PU-S4-4.

PNPs composites with different amounts (PU-S4-1 and PU-S4-2) are shown in Figures 16 and 17, and the fracture surfaces of PU/m-PNPs composites with different amounts (PU-S4-3 and PU-S4-4) are shown in Figures 18 and 19.

The low magnification images (Figure 15) show random and irregular different sizes of caves or ruptured surfaces as well as a thick layer of PU that covers the cells in some areas, indicating some degree of phase adhesion and relatively smooth fracture surface. Moreover, this phenomenon can be seen in PU-S4-1 composite that has 2.5 wt.% of PNPs, while it is different when PNPs content increases up to 5 wt.% (PU-S4-2) or when PNPs are modified with amine salts PU-S4-3 (2.5 wt.%) and PU-S4-4 (5 wt.%).

Small quantities of PNPs in PU-S4-1 were insufficient to noticeable effect on the structure of PUR, whereas it was noticeable for more quantities (PU-S4-2), or modified PNPs (PU-S4-3 and PU-S4-4) were contributed in preventing of some domains to be soft because of the effective surface of nanomaterials forming open-cells with stable dimension and rough surface, and this is evidenced by the thickness of the ribs of the cells.

The high magnification images (Figures 17, 18, and 19) show uniformly dispersed matrix and better regular incorporation of m-PNPs. Nevertheless, for PU-S4-1, the low amount of PNPs might be covered by the polymer matrix, concerning some agglomerations that form in the polymer matrix at the higher concentrations of m-PNPs.

Apparently, the more amounts of perlite particles contributed to reconstructing the structure of the polymer matrix and forming an open cellular structure.

Energy Dispersive X-ray (EDX) analysis (Figures 15, 16, 17, 18, and 19) confirmed the presence of C, O, and N elements with ratios of 78–88%, 5.1–16.4%, and ~6.2%, respectively. The high percentage of C may be attributed to the use of bio-based polyol in the production of PURFs and PURF nanocomposites. C, O, and N are distributed completely in the field of vision scope, but at a low level and clarity for O and N due to their low amounts. The results indicate the distribution of these elements is uniform, except for the agglomeration shown in the image (Figure 19) confirms the existence of these states for larger amounts of the modified nanomaterials [40–44].

4. Conclusions

The side reactions that vegetable oils do during cooking complicate to apply in the industrial field, so it was necessary to convert the UCO into valued chemicals such as polyol through conversion to epoxide and then open the ring with DEA using an environmentally friendly catalyst. The yield of the epoxidation reaction was 50% and the ring-opening was 95%, noting the presence of an amidification reaction, which could be attributed to an excess of DEA during the reaction. The hydroxide value and viscosity of the synthesized polyol were determined around 456 ± 30 mg KOH/g and 148 mPa s, which is suitable for the preparation of rigid foams. The introduction of novel polyol at ratios of 40% and 60% contributed to increasing the effectiveness of polyurethane foam. Moreover, the foams in which petrochemical-based polyols were completely replaced by the UCO-based polyol showed an open cell structure with slightly good thermal properties. Increasing the percentage of perlite or adding modified perlite in the fully substituted rigid polyurethane foam improved its dimensional and thermal stability.

Data Availability

The datasets generated during or analyzed during the current study are available from the corresponding author on request.

Conflicts of Interest

The authors declare that they have no conflicts of interest.

Acknowledgments

The authors are grateful to University of Imam Khomeini International University (IKIU), which supported this work.

References

[1] R. Jerome, M. Henrioulle-Granville, B. Boutevin, and J. J. Robin, "Telechelic polymers: synthesis, characterization and applications," *Progress in Polymer Science*, vol. 16, no. 5, pp. 837–906, 1991.

[2] G. Woods, *The ICI Polyurethanes Book*, Wiley, 2nd edition, November 1, 1990.

[3] M. Szycher, Ed., *Szycher's Handbook of Polyurethanes*, CRC Press, 1st edition, 1999.

[4] W. D. Woolley, J. M. Buist, and S. J. Grayson, *Fire and Cellular Polymers*, Elsevier Applied Science, 1986.

[5] M. Ionescu, *Chemistry and Technology of Polyols for Polyurethanes*, iSmithers Rapra Publishing, 2005.

[6] W. F. Carroll, "Upon further review: a commodity chemist on green chemistry," pp. 7–16, 2017, Sustainable Green Chemistry.

[7] W. Li, L. M. Huang, and Z. W. Zhao, "Case study on road landscape restoration of the underground commercial street," *In IOP Conference Series: Earth and Environmental Science*, vol. 153, pp. 1315–1755, 2018.

[8] K. Vasić, G. Hojnik Podrepšek, Ž. Knez, and M. Leitgeb, "Biodiesel production using solid acid catalysts based on metal oxides," *Catalysts*, vol. 10, no. 2, pp. 237–239, 2020.

[9] B. Schmidt, "Nanocomposite starch graft copolymers with carbon nanotubes–synthesis and flocculation efficiency," *Polimery*, vol. 65, no. 3, pp. 226–231, 2020.

[10] X. Yi, R. Dong, and N. Tang, "Development of a novel binder rejuvenator composed by waste cooking oil and crumb tire rubber," *Construction and Building Materials*, vol. 236, pp. 0618–0950, 2020.

[11] R. L. Permadani, M. Ibadurrohman, and Slamet, "Utilization of waste cooking oil as raw material for synthesis of methyl ester sulfonates (MES) surfactant," *In IOP Conference Series: Earth and Environmental Science*, vol. 105, p. 12036, 2018.

[12] M. M. Khalaf, A. H. Tantawy, K. A. Soliman, and H. M. Abd El-Lateef, "Cationic gemini-surfactants based on waste cooking oil as new 'green' inhibitors for N80-steel corrosion in sulphuric acid: a combined empirical and theoretical approaches," *Journal of Molecular Structure*, vol. 1203, p. 127442, 2020.

[13] J. O. Adebayo, M. Napiah, K. Ibrahim, and M. R. Kabit, "Evaluation of waste cooking oil as sustainable binder for building blocks," in *E3S Web of Conferences*, vol. 65, p. 5003, EDP Sciences, 2018.

[14] G. Feng, L. Hu, Y. Ma et al., "An efficient bio-based plasticizer for poly (vinyl chloride) from waste cooking oil and citric acid: synthesis and evaluation in PVC films," *Journal of Cleaner Production*, vol. 189, pp. 334–343, 2018.

[15] P. Jia, L. Hu, X. Yang, M. Zhang, Q. Shang, and Y. Zhou, "Internally plasticized PVC materials via covalent attachment of aminated tung oil methyl ester," *RSC Advances*, vol. 7, no. 48, pp. 30101–30108, 2017.

[16] J. R. Joshi, K. K. Bhanderi, and J. V. Patel, "Waste cooking oil as a promising source for bio lubricants-a review," *Journal of the Indian Chemical Society*, vol. 100820, 2022.

[17] A. Orjuela and J. Clark, "Green chemicals from used cooking oils: trends, challenges, and opportunities," *Current Opinion in Green and Sustainable Chemistry*, vol. 26, p. 100369, 2020.

[18] M. Sarim, M. M. Alavi Nikje, and M. Dargah, "Synthesis and characterization of polyurethane rigid foam by using feedstocks received from renewable and recyclable resources," *Journal of Porous Materials*, pp. 1–20, 2023.

[19] K. Uram, A. Prociak, and M. Kurańska, "Influence of the chemical structure of rapeseed oil-based polyols on selected properties of polyurethane foams," *Polimery*, vol. 65, no. 10, pp. 698–707, 2020.

[20] U. Stirna, A. Fridrihsone, B. Lazdiņa, M. Misāne, and D. Vilsone, "Biobased polyurethanes from rapeseed oil polyols: structure, mechanical and thermal properties," *Journal of Polymers and the Environment*, vol. 21, no. 4, pp. 952–962, 2013.

[21] M. Kurańska, K. Polaczek, M. Auguścik-Królikowska, A. Prociak, and J. Ryszkowska, "Open-cell rigid polyurethane bio-foams based on modified used cooking oil," *Polymer*, vol. 190, p. 122164, 2020.

[22] M. Kurańska and E. Malewska, "Waste cooking oil as starting resource to produce bio-polyol - analysis of transesteryfication process using gel permeation chromatography," *Industrial Crops and Products*, vol. 162, p. 113294, 2021.

[23] C. Descorme, P. Gallezot, C. Geantet, and C. George, "Heterogeneous catalysis: a key tool toward sustainability," *ChemCatChem*, vol. 4, no. 12, pp. 1897–1906, 2012.

[24] M. Kurańska, H. Beneš, A. Prociak, O. Trhlíková, Z. Walterová, and W. Stochlińska, "Investigation of epoxidation of used cooking oils with homogeneous and heterogeneous catalysts," *Journal of Cleaner Production*, vol. 236, p. 117615, 2019.

[25] F. Shirini, M. Mamaghani, and S. V. Atghia, "Sulfonic acid functionalized ordered nanoporous Na^+ montmorillonite as an efficient and recyclable catalyst for the chemoselective methoxymethylation of alcohols," *Journal of Nanostructure in Chemistry*, vol. 3, no. 1, pp. 1–5, 2012.

[26] L. Madaleno, R. Pyrz, A. Crosky et al., "Processing and characterization of polyurethane nanocomposite foam reinforced with montmorillonite-carbon nanotube hybrids," *Composites Part A: Applied Science and Manufacturing*, vol. 44, pp. 1–7, 2013.

[27] M. X. Ai, L. Q. Cao, X. L. Zhao, Z. Y. Xiang, and X. Y. Guo, "Preparation and characterization of polyurethane rigid foam/expanded perlite thermal insulation composites," *Advanced Materials Research*, vol. 96, pp. 141–144, 2010.

[28] B. Szadkowski, A. Marzec, P. Rybiński, W. Żukowski, and M. Zaborski, "Characterization of ethylene–propylene composites filled with perlite and vermiculite minerals: mechanical, barrier, and flammability properties," *Materials*, vol. 13, no. 3, p. 585, 2020.

[29] M. M. Alavi Nikje, A. B. Garmarudi, and M. Haghshenas, "Effect of talc filler on physical properties of polyurethane rigid foams," *Polymer-Plastics Technology and Engineering*, vol. 45, no. 11, pp. 1213–1217, 2006.

[30] N. Azgomi and M. Mokhtary, "Nano- Fe_3O_4@SiO_2 supported ionic liquid as an efficient catalyst for the synthesis of 1,3-

thiazolidin-4-ones under solvent-free conditions," *Journal of Molecular Catalysis A: Chemical*, vol. 398, pp. 58–64, 2015.

[31] M. Bouri, M. Gurau, R. Salghi, I. Cretescu, M. Zougagh, and Á. Rios, "Ionic liquids supported on magnetic nanoparticles as a sorbent preconcentration material for sulfonylurea herbicides prior to their determination by capillary liquid chromatography," *Analytical and Bioanalytical Chemistry*, vol. 404, no. 5, pp. 1529–1538, 2012.

[32] Y. Jiang, C. Guo, H. Xia, I. Mahmood, C. Liu, and H. Liu, "Magnetic nanoparticles supported ionic liquids for lipase immobilization: enzyme activity in catalyzing esterification," *Journal of Molecular Catalysis B: Enzymatic*, vol. 58, no. 1–4, pp. 103–109, 2009.

[33] C. P. Mehnert, R. A. Cook, N. C. Dispenziere, and M. Afeworki, "Supported ionic liquid catalysis–a new concept for homogeneous hydroformylation catalysis," *Journal of the American Chemical Society*, vol. 124, no. 44, pp. 12932–12933, 2002.

[34] M. M. A. Nikje, M. A. F. Nejad, K. Shabani, and M. Haghshenas, "Preparation of magnetic polyurethane rigid foam nanocomposites," *Colloid and Polymer Science*, vol. 291, no. 4, pp. 903–909, 2013.

[35] M. M. A. Nikje, F. Abedinifar, and A. Idris, "Epoxidized soybean oil ring opening reaction under MW irradiation," *Applied Science Research*, vol. 3, pp. 383–388, 2011.

[36] L. Moradi and M. Mirzaei, "Immobilization of Lewis acidic ionic liquid on perlite nanoparticle surfaces as a highly efficient solid acid catalyst for the solvent-free synthesis of xanthene derivatives," *RSC Advances*, vol. 9, no. 35, pp. 19940–19948, 2019.

[37] M. M. A. Nikje, R. G. Kalishomi, and R. Akbar, "Preparation of polyurethane flexible foam nanocomposites by incorporation of Fe_3O_4 nanoparticles modified by reaction product of GPTS and APTS," *Cellular Polymers*, vol. 34, no. 5, pp. 249–264, 2015.

[38] É. S. Oliveira, J. M. F. de Almeida, E. D. Junior, and N. S. Fernandes, "Evaluation of the applicability of thermogravimetry in the monitoring of the organofunctionalization process of expanded perlite," *Thermochimica Acta*, vol. 672, pp. 107–117, 2019.

[39] P. Parcheta and J. Datta, "Structure analysis and thermal degradation characteristics of bio-based poly (propylene succinate) s obtained by using different catalyst amounts," *Journal of Thermal Analysis and Calorimetry*, vol. 130, no. 1, pp. 197–206, 2017.

[40] M. M. A. Nikje and A. Yaghoubi, "Preparation and properties of polyurethane/functionalized multi-walled carbon nanotubes rigid foam nanocomposites," *Polimery*, vol. 59, no. 11/12, pp. 776–782, 2014.

[41] S. A. Shokry, A. K. El Morsi, M. S. Sabaa, R. R. Mohamed, and H. E. El Sorogy, "Synthesis and characterization of polyurethane based on hydroxyl terminated polybutadiene and reinforced by carbon nanotubes," *Egyptian Journal of Petroleum*, vol. 24, no. 2, pp. 145–154, 2015.

[42] S. S. Gedam, A. K. Chaudhary, R. P. Vijayakumar, A. K. Goswami, G. S. Bajad, and D. Pal, "Thermal, mechanical and morphological study of carbon nanotubes-graphene oxide and silver nanoparticles based polyurethane composites," *Materials Research Express*, vol. 6, no. 8, article 085308, 2019.

[43] Y. Liu, J. Ma, T. Wu et al., "Cost-effective reduced graphene oxide-coated polyurethane sponge as a highly efficient and reusable oil-absorbent," *ACS Applied Materials and Interfaces*, vol. 5, no. 20, pp. 10018–10026, 2013.

[44] T. Zhang, F. Zhou, L. Hang et al., "Controlled synthesis of sponge-like porous Au–Ag alloy nanocubes for surface-enhanced Raman scattering properties," *Journal of Materials Chemistry C*, vol. 5, no. 42, pp. 11039–11045, 2017.